Bull. Mater. Sci., Vol. 37, No. 3, May 2014, pp. 371–381. © Indian Academy of Sciences.

Studies on interfacial interactions of TiO_2 nanoparticles with bacterial cells under light and dark conditions

SWAYAMPRAVA DALAI, SUNANDAN PAKRASHI, SUJAY CHAKRAVARTY†, SHAMIMA HUSSAIN†, N CHANDRASEKARAN and AMITAVA MUKHERJEE*

Centre for Nanobiotechnology, VIT University, Vellore 632 014, India
†UGC-DAE CSR, Kalpakkam Node, Kokilamedu 603 104, India

MS received 3 May 2013

Abstract. **The probable underlying mechanism(s) of bacterial cell–TiO_2 nanoparticles (TiO_2 NPs) interaction in the absence of photo-irradiation has been less studied since most of the prior cytotoxicity studies focused on irradiated TiO_2. The present study draws attention to the possible role of cell surface–TiO_2 NP interactions under dark conditions, through an array of spectroscopic and microscopic investigations. A dominant freshwater bacterial isolate, *Bacillus licheniformis*, which interacted with environmentally relevant concentrations of TiO_2 NPs (1 μg/mL), was analysed and compared under both light and dark conditions. Aggregation of cells upon NP interaction and adsorption of NPs onto the cell membrane was evident from the scanning electron micrographs under both light and dark conditions. The FT–IR and FT–Raman spectra suggested stress response of bacterial cells by elevated protein and polysaccharide content in the cell–NP interaction. The X-ray photoelectron spectroscopic data substantiated the reduction of titanium from Ti(IV) to Ti(III) species which might have contributed to the redox interactions on the cell surface under light as well as dark conditions. The internalization of NPs in the cytoplasm were obvious from the transmission electron micrographs. The consequent cell death/damage was confirmed through fluorescence spectroscopy and microscopy. To conclude, the current study established the substantial role of interfacial interactions in cytotoxicity of the TiO_2 NPs irrespective of the irradiation conditions.**

Keywords. **Cytotoxicity; dark; FT–IR; FT–Raman; XPS; fluorescence spectroscopy.**

1. Introduction

Metal oxide nanoparticles with unique physicochemical properties are on the move, having various industrial applications in the field of sensors, ceramics, absorbents and/or catalysts. Most innovations or novel applications of these NPs are based on the size dependent optical, mechanical and chemical (reduction/oxidation) properties (Fernández-García and Rodriguez 2011). Titanium dioxide NPs are currently among the most used nanomaterials with major applications as photocatalysts and adsorbents (Liang *et al* 2001; Fujishima *et al* 2010). These NPs are widely exploited in cosmetic industry as sunscreen products, as food additives, as a catalyst and as an adsorbent in waste water treatment (Meng *et al* 2005; Pena *et al* 2005). TiO_2 NPs are stable in aqueous media and are tolerant to both acidic and alkaline conditions. In consequence of the increasing demand, these NPs are posing a threat to contaminate the aquatic environment if not disposed properly (O'Brien and Cummins 2010).

Though the phototoxic activity of TiO_2 NPs is quite well explored (Aruguete and Hochella Jr 2010; Jiang *et al* 2011), a handful of studies are available probing the possible toxicity mechanisms of TiO_2 NPs in the absence of irradiation (Adams *et al* 2006). Though generation of reactive oxygen species (ROS) was revealed to be the foremost reason for TiO_2 toxicity under light conditions (Neal 2008), the fundamental mechanism describing cytotoxicity under dark is still not clear. In a bacterial system, Zhukova *et al* (2010) have reported aggregation of *Escherichia coli* cells and suppression of their cell division in presence of TiO_2 NPs, under dark conditions. Few researchers have given a direct evidence for the free radical formation at the TiO_2 NP surface irrespective of irradiation with UV light (Sayes *et al* 2006; Fenoglio *et al* 2009). In our previous report (Dalai *et al* 2012), we have shown two possible pathways under light and dark conditions leading to cytotoxicity of TiO_2 NPs, on a freshwater bacterial isolate.

Cell–nanoparticle interactions may give rise to a number of interfaces between nanoparticles and cell and cell constituents such as organelles and DNA. These biophysico-chemical interactions may induce phase transformation of biomolecules at the cell surface and also

*Author for correspondence (amit.mookerjea@gmail.com)

may lead to nanoparticle surface modification or dissolution (Nel *et al* 2009). Exploring various interfacial interactions can be helpful in understanding the relationship between nanoparticle properties and its activity. FT–IR and FT–Raman spectroscopy are highly classified techniques to identify any chemical or structural changes in the macromolecules and hence will be very much helpful in understanding cell–nanoparticle interactions (Schuster *et al* 2000; Wang *et al* 2012). Possible redox reactions at the cell–NP interface involving reduction of Ti(IV) to Ti(III) species can be confirmed using X-ray photoelectron spectroscopy (XPS) (Rtimi *et al* 2012). Microscopic techniques such as confocal and atomic force microscopy (AFM) have also been applied to study the complex interfacial interactions (Wang *et al* 2012; Li Kungang *et al* 2013). A detailed literature survey reveals an acute lack of mechanistic understanding with regard to the dynamic chemical environment involving the complex surface reactions at the critical cell–NP interface, especially under dark/non-irradiated conditions. Hence, the current study focuses on elucidating the bio-physico-chemical interactions at cell–NP interface using spectroscopic (FT–IR, FT–Raman, XPS and fluorescence spectroscopy) and microscopic (SEM, TEM, fluorescence microscopy) techniques as key tools.

2. Materials and methods

2.1 *Chemicals*

TiO_2 nanoparticles were procured from Sigma Aldrich; Supplier's data: dry titanium (IV) dioxide nanopowder, 99·7% anatase, particle size: < 25 nm, CAS no.: 637254. Propidium iodide (PI) (P4170–10MG; ≥ 94%) was purchased from Sigma Aldrich. All other chemicals used were of analytical grade.

2.2 *Experimental set up*

The dominant bacterial isolate from fresh water (VIT lake water, Vellore, India) was identified as *Bacillus licheniformis* (gram positive, rods) through 16S rRNA analysis (length of the sequence, 1462 bp; homology, 99%). Bacteria with cell count of 5×10^8 CFU/mL were interacted with TiO_2 NPs (concentration: 1 μg/mL) for an exposure period of 2 h. All the biological experiments were carried out under light (UV-irradiation, wavelength < 390 nm) and dark (no irradiation) conditions. For light experiments, continuous UV irradiation was provided by incandescent light bulbs (15 lm/W, Philips, India), and for dark experiments, samples were kept in dark rooms and covered with opaque sheets to avoid any intervention of light during handling. Sterile lake water was used as the experimental matrix. Hydrodynamic diameter of NPs dispersed in lake water (concentration: 1 μg/mL) was measured using particle size analyzer (90 plus Particle Size Analyser, Brookhaven Instruments Corporations, USA).

2.3 *Photocatalytic activity of TiO_2 NPs*

The procured TiO_2 NP was characterized using UV-Probe/DRS (UV-2600, Shimadzu, Germany). The reflectance diffusion spectrum and the absorption spectrum were obtained and analysed for confirming the photo absorption of NPs ((details in Supplementary Information).

In order to evaluate the photocatalytic activity of TiO_2 NPs, production of intracellular reactive oxygen species (ROS) in presence and absence of UV-irradiation was measured. Five millilitre of TiO_2 NP dispersion (1 μg/mL) was prepared in the experimental matrix and kept in light and dark conditions, respectively for a period of 2 h. After the exposure period, the dispersion was incubated with 100 μM DCFH-DA for 30 min under dark conditions, following the protocol of Wang and Joseph (1999). Spectrofluorometer (SL174, ELICO, India) with excitation and emission wavelengths of 485 and 530 nm, respectively was used for the analysis. Two different control samples were also taken (one each for light and dark conditions). The fluorescence intensity of control sample was considered as 0% and the respective percentage intensity was calculated for test samples.

2.4 *Zeta potential analysis*

Surface charge (zeta potential) of cell and NPs was measured to find out the possibilities of any charge based interaction. The bacterial cells were interacted with TiO_2 NPs (1 μg/mL) under light and dark conditions and the net charge on NPs, bacterial cells and NP-interacted cells were estimated using zeta analyser (90 plus particle size analyser with zeta option, Brookhaven Instruments Corporations, USA).

2.5 *Scanning electron microscopy (SEM)*

Morphological variation of cells, their aggregation and NP attachment onto the membrane was observed under scanning electron microscope (SEM). Aliquots of bacterial cell suspensions interacted with 1 μg/mL of TiO_2 NPs (along with control) were withdrawn after 2 h of the experimental period. A thorough washing of the cells was done with phosphate buffered saline (PBS) to remove loosely adsorbed NPs. A drop of the cell suspension was placed on the cover slip and air dried. Chemical fixation with 4% (w/v) glutaraldahyde was done for a period of 24 h followed by ethanol dehydration. The dried bacterial film was gold sputtered and loaded for SEM analysis (Model S400, Hitachi).

2.6 *FT–IR analysis*

Any alteration in surface chemistry of bacterial cells upon NP interaction (1 μg/mL) was confirmed by Fourier–transform infrared spectroscopy (FT–IR). Five millilitre of the cell suspension after 2 h interaction period was centrifuged for 10 min at 7000 g. The pellet was washed twice with 1 mL PBS and lyophilized to remove moisture. The dried cells were then subjected to FT–IR analysis by KBr technique (Nicolet 6700 FT–IR spectrometer, Thermo Scientific Instruments Groups, Madison, Wisconsin).

2.7 *FT–Raman analysis*

To confirm the FT–IR analysis, FT–Raman study was carried out. After interaction with NPs (1 μg/mL, 2 h), the lyophilized cells (control and interacted) were subjected to FT–Raman analysis using BRUKER RFS 27: stand alone FT–Raman spectrometer. The spectrum range scanned was 50–4000 cm^{-1} and the spectral resolution was 2 cm^{-1}.

2.8 *X-ray photoelectron spectroscopy (XPS) analysis*

The chemical states of titanium, after interaction with bacterial cells, were studied by X-ray photoelectron spectroscopy (XPS). Lyophilized, NP interacted bacterial cells (with NP concentration, 1 μg/mL) and uninteracted cells were made into pellets (5 × 1 mm) and subjected to XPS analysis (details in Supplementary Information).

2.9 *Transmission electron microscopy (TEM)*

Internalization and localization of NPs in the cell and changes in cellular structure were observed by TEM (Philips CM12 transmission electron microscope, The Netherlands) (details in Supplementary Information).

2.10 *Inductively coupled plasma–optical emission spectroscopy (ICP–OES) analysis*

The amount of TiO_2 NP present at the cellular interior was quantified by ICP–OES (Perkin Elmer Optima 5300 DV, USA) analysis. Five millilitres of bacterial sample (1 μg/mL, 2 h) were centrifuged (4000 g for 20 min) and the supernatant was separated. Pellet was resuspended in 5 mL of EDTA (0·02 M) and gently inverted for 30 s to remove the extracellular NPs (Beletsky and Umansky 1999). Centrifugation (4000 g, 20 min) was done and the supernatant containing extracellular NPs was separated. The pellet (now containing only internalized NPs) was acid digested with excess of conc. HCl and filtered with Whatman no. 1 filter paper. After external calibration, analysis was carried out at a wavelength of 334·94 nm for the metal Ti.

2.11 *Fluorescent microscopy and spectroscopy*

NP uninteracted and interacted cells stained with propidium iodide (PI) were observed under microscope (details in Supplementary Information). Spectrofluorometric analysis was done to quantify the dead/damaged cells in the interacted sample following the protocol described by Beletsky and Umansky (1990) with little modifications. Interacted and uninteracted cells (5 mL) were stained with 300 μL of PI and incubated for 5 min. A three-step washing with 2 × SSC buffer was done and spectrofluorometric analysis was performed (spectrofluorometer, SL174, ELICO) with excitation wavelength of 536 nm and emission wavelength of 617 nm. Fluorescence intensity was calculated for the un-interacted and the interacted samples. The analyses were performed in triplicate to ensure reproducibility of the experiment.

2.12 *Statistical analysis*

Statistical analysis of ROS assay, quantified metal ions and fluorescence intensity of interacted and uninteracted samples was carried out using paired *t*-test (parametric) at $P < 0{\cdot}05$. Graph pad prism (Version 6·01) was used for all the statistical analyses.

3. Results and discussion

The physicochemical characterization of sterilized freshwater is as follows: conductance: 4·5 ± 0·17 mS/cm; pH: 7·7 ± 0·2; dissolved oxygen: 7·4 ± 0·49 μg/mL; total dissolved solids: 820 ± 80 μg/mL. The lake water was found to contain trace amount of basal metal ions such as Al^{3+}, Cu^{2+}, Zn^{2+}, Mn^{2+} (confirmed from ICP-OES analysis) and inorganic ions such as SO_4^{2-}, PO_4^{3-}, NO_3^-, Cl^- (confirmed from titrimetric analysis).

3.1 *Photocatalytic activity, particle size and surface charge*

The characteristic DRS spectra of TiO_2 NPs (figure 1) confirmed its optical response of UV irradiation. The photocatalytic activity of TiO_2 NPs was confirmed by ROS assay under UV-light and dark conditions. TiO_2 NP dispersion in sterile lake water was subjected to light and dark reaction conditions for 2 h and the respective ROS production was quantified. The percentage generation of ROS was noted to be 0·982 ± 0·13% and 0·041 ± 0·004% under light and dark conditions, respectively with regard to control (considered as 0 ± SE%). The significant ROS

production ($P < 0{\cdot}05$), under UV-irradiation condition thus confirmed photocatalytic activity of TiO_2 (anatase) NPs.

The TiO_2 NP dispersion in lake water matrix was found to be stable during the experimental period (Dalai *et al* 2012). The hydrodynamic diameter of particles was found to be in the range of 50–200 nm with mean particle size, 78 nm.

To establish an understanding with regard to charge based interaction of bacterial cells and NPs under both light and dark conditions, zeta potential analysis was carried out. The zeta potential value for bacterial cells was noted to be $-28{\cdot}5 \pm 0{\cdot}48$ mV and that for NPs $-20{\cdot}7 \pm 1{\cdot}5$ mV, which suggests no average surface charge based interaction of cell and NPs. A study by Beveridge *et al* (1982) demonstrated that bacterial cell surface is typically anionic and *B. licheniformis* cell walls can bind positive metal ions strongly, where the teichoic acid–peptidoglycan complex plays a major role. Fang *et al* (2010) demonstrated the cytotoxic potential of several NPs towards *Nitrosomonas europaea*, irrespective of their size and surface charge. Hence, NP surface charge is not a limiting factor for deciding its cytotoxicity potential and consequently, the possible role of localized cationic charge densities on NP surface and presence of phosphate, amide, carbohydrate related moieties on the cell surface, in cell–NP interaction, could not be neglected.

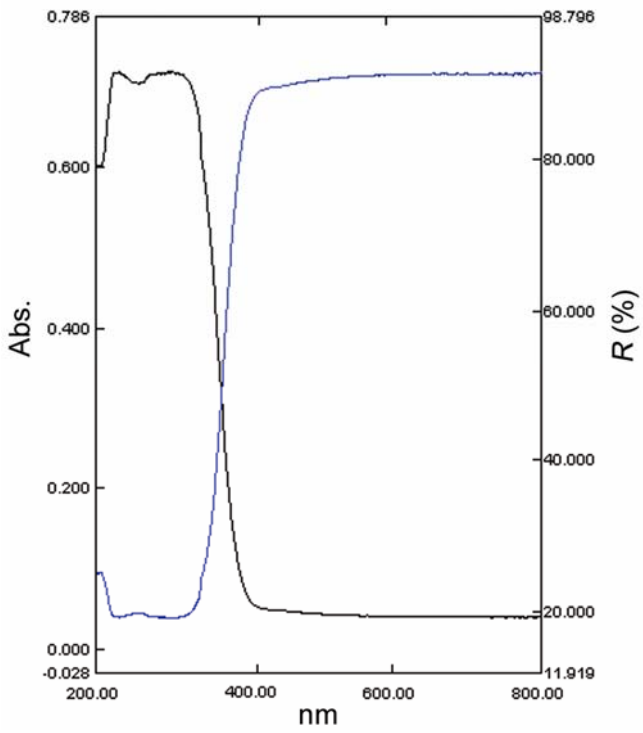

Figure 1. UV/DRS spectra of as received TiO_2 NPs showing absorption (black) and reflectance (blue) spectra.

3.2 *Surface attachment: scanning electron microscopy*

The smooth surface of control/untreated cells were observed under scanning electron microscopy (figure 2(a)). On the other hand, roughening of cell surface was noted due to attachment of NPs onto cell membrane in case of both light and dark interacted cells (figures 2(b and c)). The cells were found to have a tendency to aggregate within a few hours interaction (figure 2(d)). Surface attachment of NPs into the cells was confirmed by ICP-OES analysis. After the interaction period, the surface attached Ti content presumably owing to the adhesion of the NPs, was quantified to be $0{\cdot}371 \pm 0{\cdot}032$ and $0{\cdot}393 \pm 0{\cdot}053$ μg mL^{-1} under light and dark conditions, respectively. No Ti content was observed in the uninteracted cells. These data suggested comparatively more NP adsorption onto the cell surface in dark treated samples. Our previous study on TiO_2 NP and bacteria interaction (Dalai *et al* 2012) corroborated with this particular observation. Similar observations were also reported by Zukova *et al* (2010) showing aggregation of *E. coli* cells at pH 4–4·5 in the absence of UV irradiation. The shape and structure changes of the bacterial cells such as *Bacillus subtilis*, *Acinetobacter junii* and *E. coli* upon heavy metal (Cr(VI)) stress were also evidenced by Samuel *et al* (2012).

SEM observations persuaded us to explore the mechanistics of the complex interfacial phenomena at the cell–NP interface, which may facilitate the possible uptake/internalization of the NPs in the cytoplasm.

3.3 *Surface chemistry: FT–IR*

FT–IR analysis was done to find out the possible changes in surface chemistry of bacterial cells after NP interaction. FT–IR band assignments have been made based on reported values for the various functional groups for bacterial cells (Nakamoto *et al* 1963; Maquelin *et al* 2002). FT–IR spectrum of TiO_2 NPs (Sadiq 2011) was contrasted with the spectra obtained with bacterial samples. FT–IR spectra for control and NP interacted bacterial samples was compared (figure 3). Notably, the control sample spectrum showed a shoulder formation at 1736 cm^{-1} which represents ν(C=O) in polyester compounds and the band at 1162 cm^{-1} which can be assigned to C–O stretching vibrations in polysaccharides. A peak at 1644 cm^{-1} denotes amide-I groups as expected for bacterial cultures. A characteristic peak attributed to phospholipids on the cell membrane (PO^{2-} vibrations) was evident at 1230 cm^{-1} (Liu *et al* 2011). A broad and smooth fingerprint region (900–600 cm^{-1}) region was noted in control samples which eventually became distorted upon NP interaction.

After treating the bacterial cells with nanoparticles, the following changes were observed under both light and

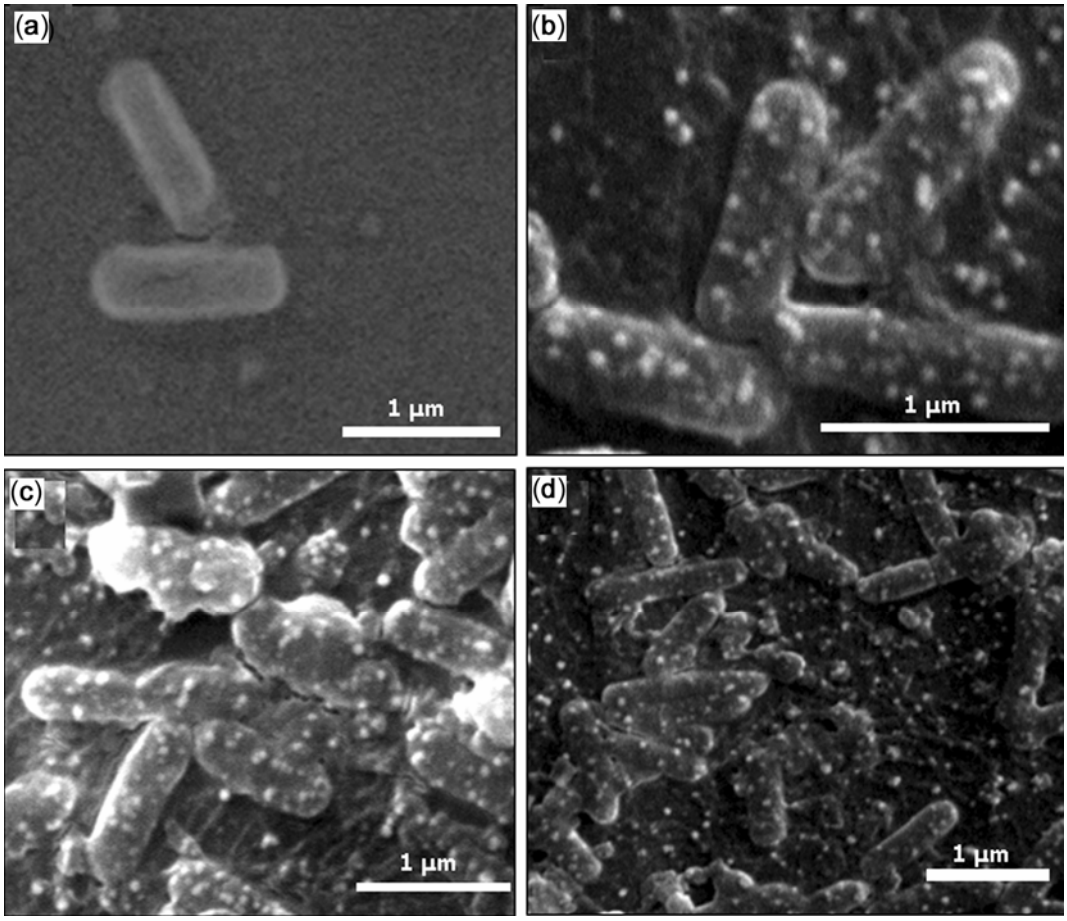

Figure 2. Scanning electron micrograph of (**a**) uninteracted cells; (**b**) NP interacted cells under light conditions; (**c**) NP interacted cells under dark conditions and (**d**) aggregation of cells after NP interaction, under dark conditions.

dark conditions. A considerable increase in peak intensity was observed at ~ 1640–1650 cm^{-1} which denoted amide-I group and hence increased cellular protein content. Also in dark treated samples, more intense peak and a slight shift in band position (1644–1648 cm^{-1}, amide-I) was observed suggesting elevated protein content. A completely new peak at ~ 1550 cm^{-1} was observed in both the interacted samples (amide-II), confirming raised protein level under stress conditions. A shoulder formation at 2854, 2924 and 2958 cm^{-1} was observed in interacted bacteria showing increased fatty acid content. A band at about 1736 cm^{-1} in control cells disappeared upon NP interaction suggesting possible involvement of >C=O stretch of polyesters. Appearance of additional peaks at about 1400 cm^{-1} showed increased level of carboxylic acid (COO^-) in interacted samples, suggesting higher level of fatty acids. The peak at about 1230 cm^{-1} may be attributed to the elevated level of phospholipids. A major change was also observed at the fingerprint region (900–600 cm^{-1}) in NP interacted samples. The peak positions in the range of 500–600 cm^{-1} denoted by Ti–O–Ti band appeared in the range of showing possible nanoparticle attachment to the cell wall (Pandey *et al* 2010). In dark interacted samples, the fingerprint region was comparatively more distorted than the light interacted cells suggesting the likelihood of more NP attachment on the bacterial cell wall. Hence, from the above observations, it can be concluded that upon NP interaction a noteworthy surface modification is taking place which indicated stress on the microorganisms in terms of elevated protein and polysaccharide levels (Hecker and Völker 2001). To confirm the results obtained in FT–IR analysis, FT–Raman study was done.

3.4 *Surface chemistry: FT–Raman*

FT–Raman analysis of TiO_2 NP interacted and uninteracted bacterial cells, under light and dark conditions, were compared (figure 4). FT–Raman peak assignments were done based on FT–Raman database (De Gelder *et al* 2007). The major difference observed was the appearance of an extra peak at about 2930 cm^{-1} (nCH_2) in both the interacted samples showing increased lipid content.

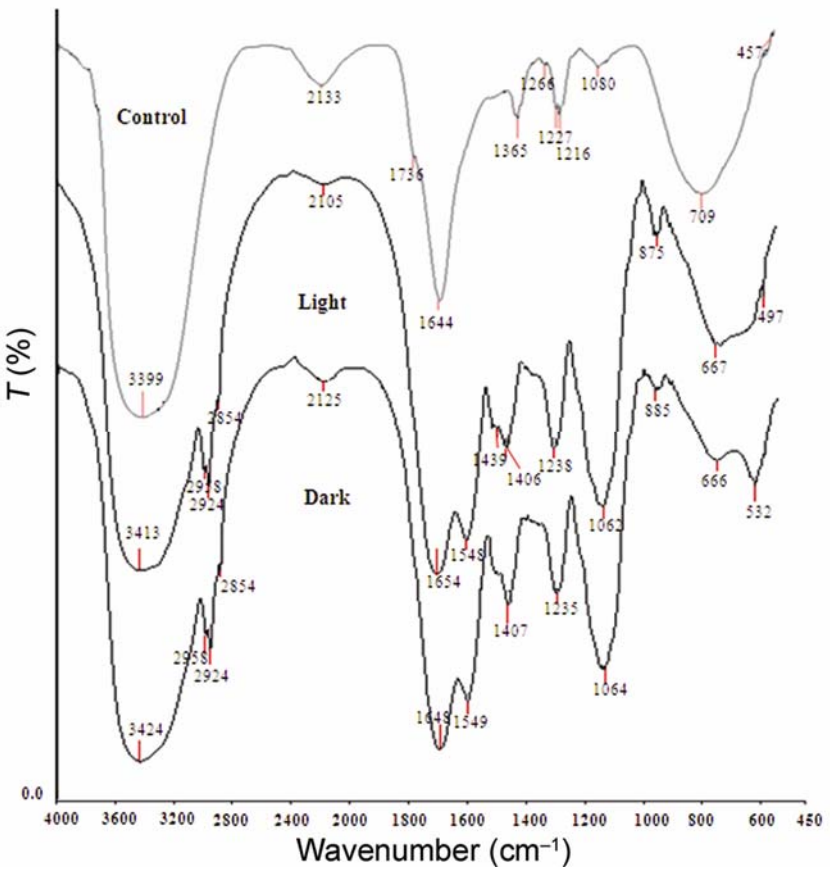

Figure 3. FT–IR spectra of control cells; NP interacted cells under light conditions and NP interacted cells under dark conditions.

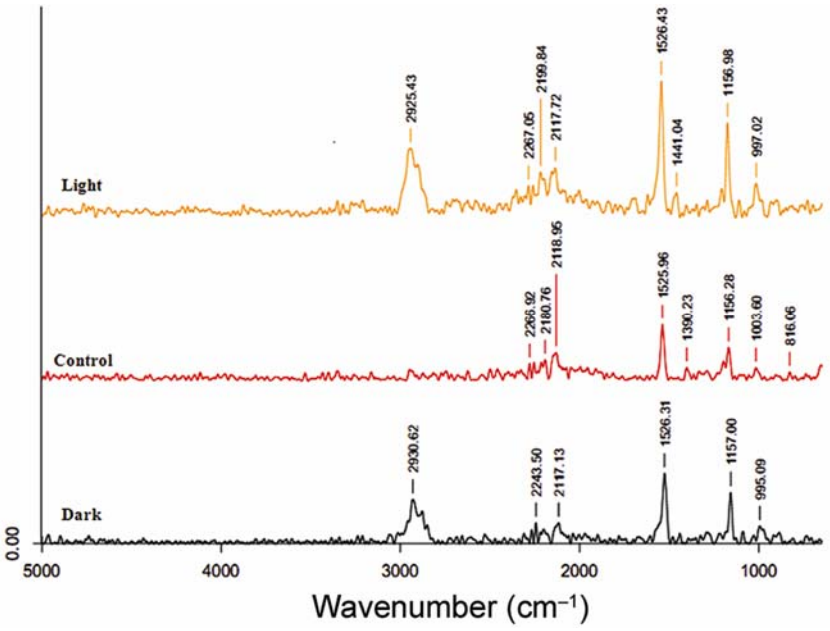

Figure 4. FT–Raman spectra of control cells (red), NP interacted cells under light conditions (orange) and NP interacted cells under dark conditions (black).

Increased intensity at ~ 1670 cm^{-1} in light and dark interacted samples suggested presence of amide-I group, which confirms elevated protein level as detected from FT–IR (Maquelin *et al* 2002). Increased peak intensity in interacted samples at about 1000 cm^{-1} can be attributed to the increased fatty acid content (phenylalanine) in interacted cells. Another intense peak in test samples at 1156 cm^{-1} suggested C–C bond in pyranose ring of increased polysaccharides. The peak regions at 858 and 1098 cm^{-1} are the molecular markers denoting the degradation of bacterial cell walls. These finger print bands highly agree with the FT–IR band observations. Higher intensities were observed in these regions in the interacted samples showing cellular damage upon NP interaction.

3.5 *Surface reactivity: XPS*

XPS analysis is a direct way for evaluating the surface reactivity of TiO_2 NPs where reduction of Ti(IV) to Ti(III) species can be confirmed. Figure 5 shows XPS spectrum of Ti 2*p* from the TiO_2 interacted bacterial cell surfaces under both light and dark conditions. The formation of Ti(III) species was confirmed from XPS analysis in both light and dark treated samples suggesting the possibility of redox reactions in the NP–cell interface. The interfacial reduction of TiO_2 NPs from Ti(IV) to Ti(III) species may lead to oxidative degradation of cell membrane, which is probably one of the major factors supporting cytotoxicity potential of these NPs (Biesinger *et al* 2010). In an experiment on bactericidal property of TiN–TiO_2 films, Rtimi *et al* (2012) reported an increase in the Ti(III) species concentration substantiating the role of redox reactions taking place during the process. In addition to the formation of Ti(III) species, interaction of TiO_2 NPs with bacterial cells may also generate free radicals. Recently, Lipovsky *et al* (2012) demonstrated free radical generation in non-illuminated TiO_2 through EPR/ESR study. Thus, the generation of free radicals and Ti(III) species confirmed the occurrence of redox reactions at the cell–NP interface which indirectly proved oxidative disruption of cellular membrane. Hence, this will facilitate the uptake/internalization of the NPs into the cells. Transmission electron microscopy and ICP-OES were done to confirm presence of NPs in the cytoplasm.

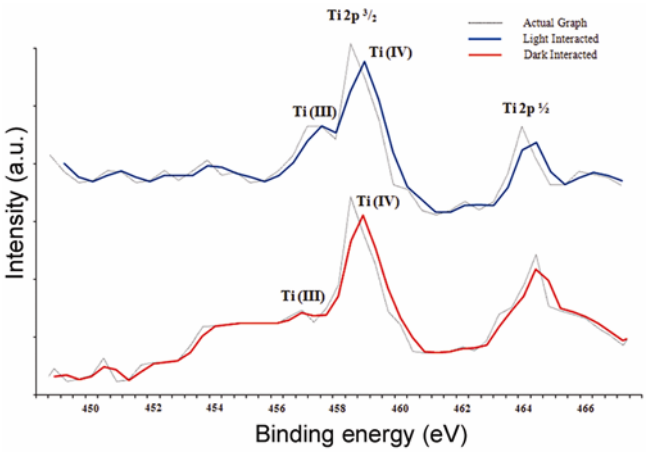

Figure 5. XPS Ti 2*p* spectra of TiO_2 interacted cells under light and dark conditions. Actual graphs are represented as dashed lines (….). Solid lights represent two-period moving average trend lines for light (blue) and dark (red) interacted samples.

3.6 *Internalization and uptake: TEM, ICP-OES*

From the above mentioned findings, it is clear that NP attachment onto the cells is one of the major reasons for cytotoxicity. The uptake/internalization of NPs in the cell was studied through transmission electron microscopy. TEM micrographs showed evenly stained interior and smooth outer surface in uninteracted cells (figure 6(a)). But, upon interaction with the NPs, the emergence of small vacuole like structures was noticeable giving a patchy appearance to the cells (figure 6(b)). In the light and dark treated samples, jagged cellular interior was evident (figures 6(c and d)). The clumps observed in interacted cells can possibly be the depositions of NPs in the cytoplasm, which may suggest internalization of NPs. Similar observations were reported by Kumar *et al* (2011) in *Escherichia coli* TiO_2 NP interaction under light conditions.

The intracellular metal (Ti) quantification data showed the presence of 0·127 ± 0·002 and 0·067 ± 0·019 $\mu g\ mL^{-1}$ ($P < 0{\cdot}05$) of titanium, presumably due to internalization of TiO_2 NPs respectively, under light and dark conditions. The control cells showed no titanium content inside the cells. ICP-OES analysis has been carried out by Zhu *et al* (2010) to quantify the bioaccumulation of TiO_2 NPs in cells in a daphnia-zebra fish food chain experiment. Considerably, more internalized NPs under light conditions point towards the phototoxic nature of TiO_2 NPs. This can be related to the oxidative dissolution of the cell membrane upon NP interaction in association to the reduction of Ti(IV) as evidenced in the previous section. Similar observations were reported by Kumar *et al* (2012) in *Escherichia coli* TiO_2 NP interaction under light conditions.

3.7 *Cellular damage/cytotoxicity: fluorescent microscopy and spectroscopy*

The internalization of the particles within the cytoplasm is bound to have toxic impact on the bacteria. To find out the toxic potential of NPs towards bacterial cells, live/dead discrimination of cells was done with PI

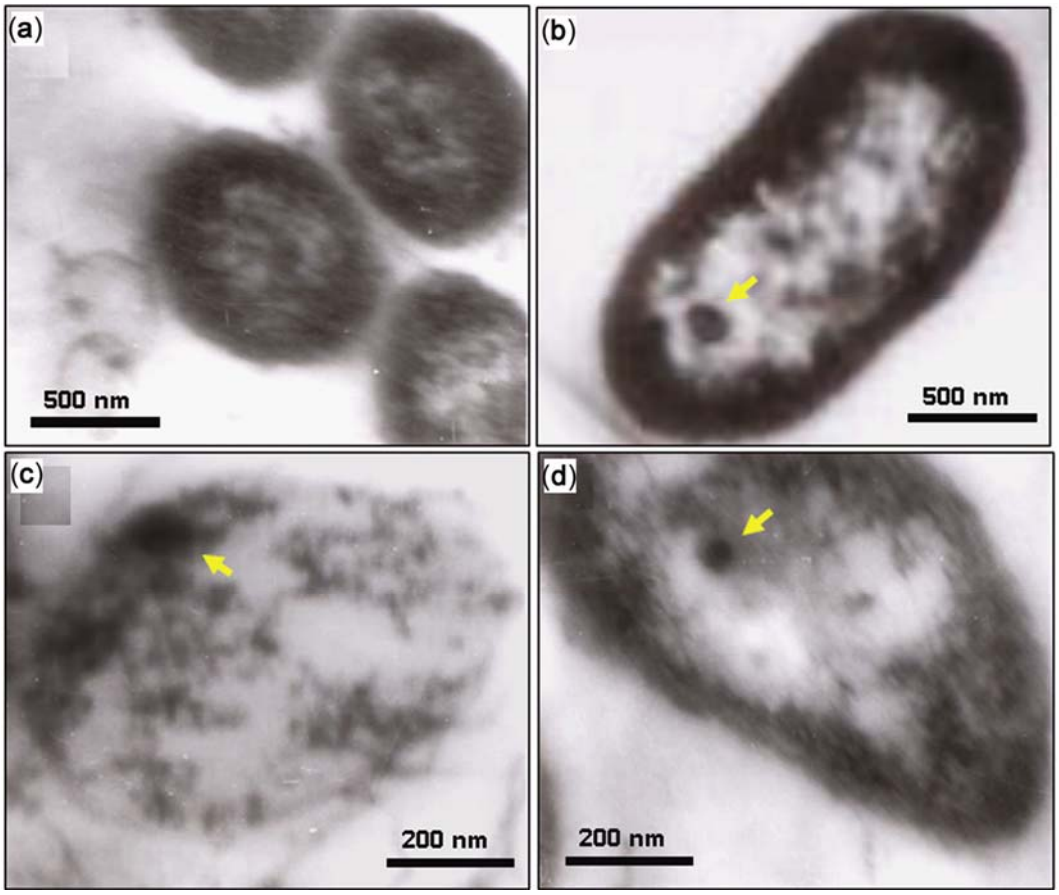

Figure 6. Transmission electron micrograph of (**a**) uninteracted cells (cross-section) showing smooth morphology; (**b**) interacted cells (longitudinal section) under dark conditions showing aggregation of NPs in cytosol; (**c**) interacted cells (cross-section) under light conditions showing NP aggregation at cell wall; (**d**) distorted cell interior and clumping of NPs in cytosol under dark conditions (yellow arrows point to aggregated NPs).

staining. Since PI is membrane impermeable, it can stain only dead or damaged cells in the sample. In the control sample, very few cells were found to have taken up the dye (figure 7(a)). In the interacted sample (1 μg/mL, 2 h), a number of cells were observed to be stained red with PI. Interestingly, the cells were noticed to form chains upon NP interaction in treated samples (figures 7(b and c)). The chain formation, which takes place due to interruption between septation and cell separation, was reported in *Bacillus* species (Guieros-Filho 2007). Forsberg *et al* (1973) reported the chain forming tendency of *B. licheniformis* under phosphate (PO_4^{3-}), Mg^{2+} limitation conditions and in Lytic (Lyt^-) mutants. The stained cells were also found to form clumps while the live cells were uniformly dispersed. Similar observations were noted under both light and dark conditions. Moreover, few cells having taken up the dye were seen to have motility, which suggests presence of live but damaged cells in the sample. Propidium iodide staining has been used as a standard technique for discriminating live and dead cells (Francolini *et al* 2004).

To quantify the number of damaged cells in the sample, spectrofluorometric analysis was carried out using propidium iodide staining. The uninteracted and NP-interacted (1 μg/mL, 2 h) cells were analysed for membrane permeability using spectrofluorimetry (figure 8(a)). Since PI can stain only the dead or the damaged cells, the intensity of PI in uninteracted and interacted cells was compared. TiO_2 NP alone did not show any fluorescence intensity (within 550–650 nm) after PI interaction (figure 8(a)). More intense peak was observed in dark treated samples compared to light interacted samples suggesting higher total membrane damage due to presence of both damaged and dead cells. The fluorescence spectra of light- and dark-treated samples showed intensities of $27{\cdot}23 \pm 3{\cdot}25$ and $36{\cdot}7 \pm 3{\cdot}37\%$, respectively ($P < 0{\cdot}05$) with regard to control (considered as $0 \pm$ SE%) (figure 8(b)). Spectrofluorometric analysis using propidium iodide is one of the standard methods to demonstrate cell viability and has been exploited by several researchers to quantify compromised cells in a sample (Garcia-Gonzalez *et al* 2010).

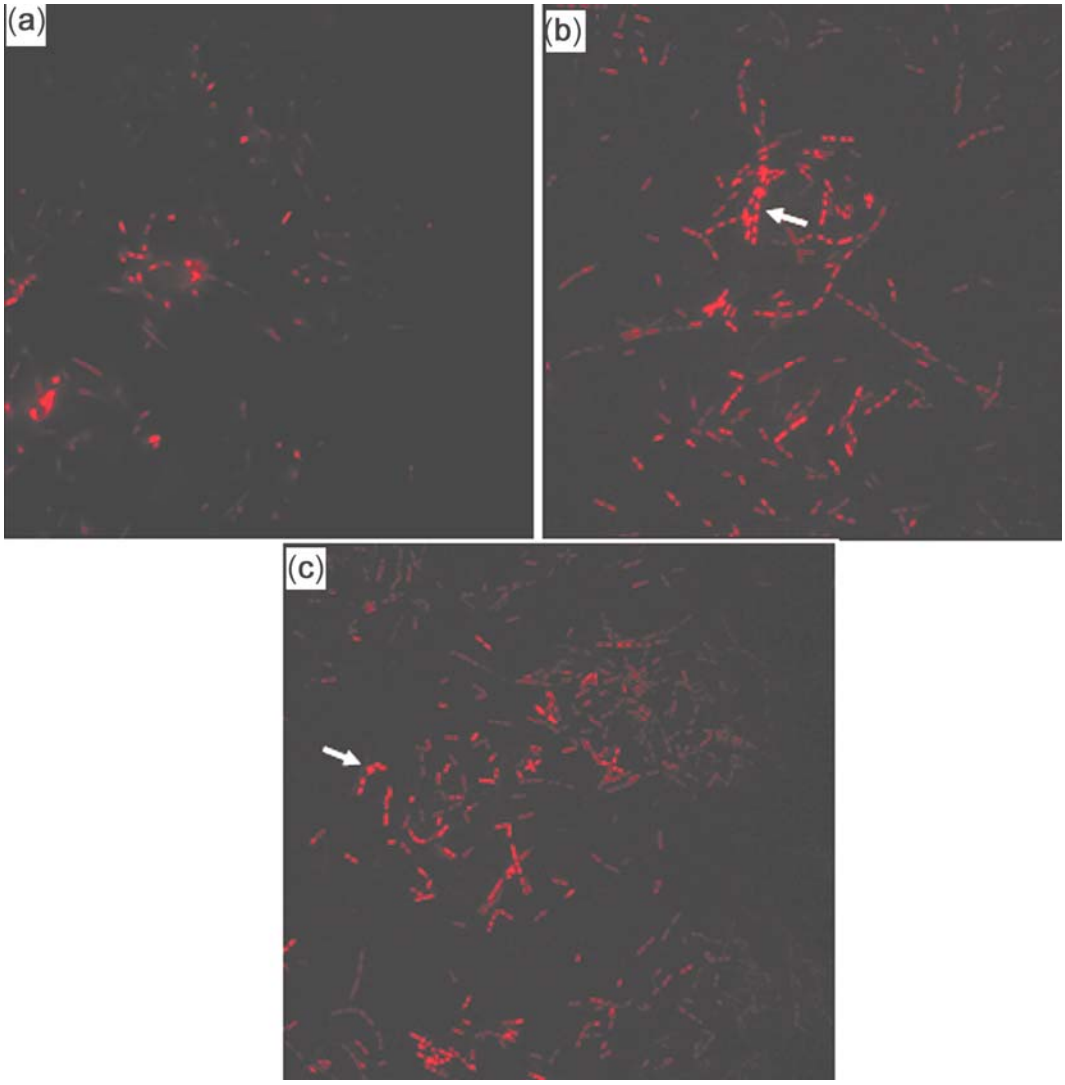

Figure 7. Fluorescence micrograph of (**a**) uninteracted cells showing few stained cells; (**b**) interacted cells under light condition showing long chained structures and (**c**) interacted cells under dark conditions showing small chained structures (White arrows depict clumping of cells).

3.8 *Possible cell/NP interfacial interactions*

In this study, we have attempted to provide spectroscopic and microscopic insight to the possible underlying mechanism of TiO_2 NP cytotoxicity under light and dark conditions. The observed cytotoxicity of TiO_2 NPs irrespective of irradiation conditions encouraged us to understand the phenomena at cell–NP interface. This cytotoxic effect is largely dependent on the stability of NPs in the matrix and its interaction with the cell surface (Pakrashi *et al* 2011). In the present study, the spectroscopic data (FT–IR and FT–Raman) showed stress response of bacterial cells upon NP interaction in terms of elevated protein and polysaccharide content both in light- and dark-treated samples. XPS study proved a partial reduction of Ti(IV) to Ti(III) species, which may contribute to the oxidative dissolution of cell membrane leading to NP internalization.

TiO_2 is well known for its phototoxicity property (Battin *et al* 2009). However, its reactivity in absence of UV-light cannot be avoided (Adams *et al* 2006). In the context of solid state physics, Burello and Worth (2011) hypothesized that the redox potential for the generation of $OH^{\bullet}$ radical species from water lies nearly at –7·4 eV, which is comparable to the valence band energy of TiO_2. Also, the probable overlapping of conduction band energy (E_c) with the biological redox potential (–4·12 to –4·84 eV) may contribute to electron transfer between NP and cells and *vice versa* (Auffan *et al* 2009; Burello and Worth 2011; Zhang *et al* 2012) leading to cytotoxicity. Hence, the excitation of electrons from valence band to conduction band does not require UV irradiation.

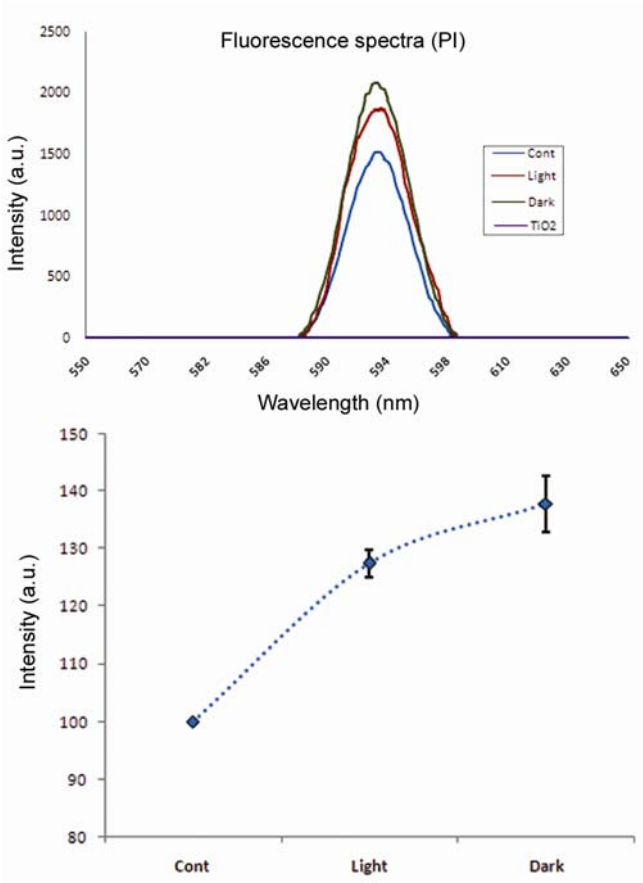

Figure 8. Fluorescence spectra of interacted cells under light condition (red), and dark condition (green). More intensity in dark interacted samples suggests presence of more damaged cells.

The potential interfacial interactions, implied from spectroscopic studies and conformed through microscopic observations, could be one of the key steps involved in the mechanism of cytotoxicity for TiO_2 NPs. A detailed study in this regard will be helpful to establish a concrete understanding of the mechanism.

4. Conclusions

The present study explores the mechanistic aspects of dynamic interfacial interactions between the bacterial cell and photocatalytic TiO_2 NP at low exposure conditions irrespective of irradiation conditions. With increasing usage of these nanoparticles as antimicrobial substances in the consumer products, mostly employing their phototoxic behaviour, non-irradiated cytotoxicity open up new vistas in their application domain. The significant findings from this study enrich the basic understanding of the fundamental surface chemistry involved in the TiO_2 NP–cell interaction especially under unirradiated conditions. Further studies need to be undertaken to gain insight into non-photocatalytic behaviour of these particles towards higher organisms and the potential cytotoxic impacts.

Electronic Supplementary Material

Supplementary material pertaining to this article is available on the Bulletin of Materials Science website (www.ias.ac.in/matersci).

References

Adams L K, Lyon D Y and Alvarez P J 2006 *Water Res.* **40** 3527

Aruguete D M and Hochella Jr M F 2010 *Environ. Chem.* **7** 3

Auffan M, Rose J, Wiesner M R and Bottero J Y 2009 *Environ. Pollut.* **157** 1127

Battin T J, Kammer F V D, Weilhartner A, Ottofuelling O and Hofmann T 2009 *Environ. Sci. Technol.* **43** 8098

Beletsky I P and Umansky S R 1999 *J. Immunol. Meth.* **134** 201

Beveridge T J, Forsberg C W and Doyle R J 1982 *J. Bacteriol.* 1438

Biesinger M C, Lau W M, Gerson A R and Smart R C 2010 *Appl. Surf. Sci.* **257** 887

Burello E and Worth A P 2011 *Nanotoxicol.* **5** 228

Dalai S, Pakrashi S, Suresh R S, Chandrasekaran N and Mukherjee A 2012 *Tox. Res.* **1** 116

De Gelder J, De Gussem K, Vandenabeele P and Moens L 2007 *J. Raman Spectrosc.* **38** 1133

Fang X, Yu R, Li B, Somasundaran P and Chandran K 2010 *J. Coll. Interf. Sci.* **348** 329

Fenoglio I, Greco G, Livraghi S and Fubini B 2009 *Chem. Eur. J.* **15** 4614

Fernández-García M and Rodriguez J A 2011 *Metal Oxide Nanoparticles. Encyclopedia Inorganic Bioinorganic Chemistry* (DOI: 10.1002/978119951438.eibc0331)

Forsberg C W, Wyrick P B, Ward J B and Rogers H J 1973 *J. Bacteriol.* **113** 969

Francolini I, Norris P, Piozzi A, Donelli G and Stoodley P 2004 *Antimicrob. Agents Chemother.* **48** 4360

Fujishima A, Rao T N and Tryk D A 2000 *J. Photochem. Photobiol.* **C1** 1

Garcia-Gonzalez L, Geeraerd A H, Mast J, Briers Y, Elst K, Van Ginneken L, Van Impe J F and Devlieghere F 2010 *Food Microbiol.* **27** 540

Guieros-Filho F J 2007 *Bacillus subtilis: Cellular and molecular biology* (ed.) Peter Graumann (Germany: Horizon Scientific Press) pp 93–134

Hecker M and Völker U 2001 *Adv. Microb. Physiol.* **44** 35

Jiang G, Shen Z, Niu J, Bao Y, Chen J and He T 2011 *J. Environ. Monit.* **13** 42

Kumar A, Pandey A K, Singh S S, Shanker R and Dhawan A 2011 *Free Radical Biol. Med.* **51** 1872

Li Kungang, Zhang W and Chen Y 2013 *Biotechnol. J.* 8

Liang Y, Gan S, Chambers S A and Altman E I 2001 *Phys. Rev.* **B63** 235402

Lipovsky A, Ievitski L, Tzitrinovich Z, Gedanken A and Lubart R 2012 *Photochem. Photobiol.* **88** 14

Liu Z, Yang S, Bai Y, Xiu J, Yan H, Huang J, Wang L, Zhang H and Liu Y 2011 *Miner. Eng.* **24** 839

Maquelin K, Kirschner C, Choo-Smith L P, van den Braak N, Endtz H P, Naumann D and Puppels G J 2002 *J. Microbiol. Meth.* **51** 255

Meng X, Dadachov M, Korfiatis G P and Christodoulatos C 2005 US Patent Application Number 6,919,029

Nakamoto K 1963 *Infrared spectra of inorganic and coordination compounds* (New York: John Wiley and Sons) p. 107

Neal A L 2008 *Ecotoxicology* **17** 362

Nel A E, Madler L, Velegol D, Xia T, Hoek E M V, Somasundaran P, Kaelssig F, Castranova V and Thompson M 2009 *Nat. Mater.* 543

O'Brien N and Cummins E 2010 *J. Environ. Sci. Health, Part A* **45** 992

Pakrashi S, Dalai S, Sabat D, Singh S, Chandrasekaran N and Mukherjee A 2011 *Chem. Res. Toxicol*. **24** 1899

Pandey R R, Saini K K and Dhayal M 2010 *J. Biosens. Bioelectron.* **1** 101

Pena M E, Korfiatis G P, Patel M, Lippincott L and Meng X 2005 *Water Res.* **39** 2327

Rtimi S, Baghriche O, Pulgarin C, Sanjines R and Kiwi J 2012 *RSC Adv.* **2** 8591

Sadiq I M 2011 *Ecotoxicological studies of engineered oxide nanoparticles*, Ph D Thesis, VIT University, Vellore

Samuel J, Paul M L, Mrudula P, Joyce Nirmala M, Chandrasekaran N and Mukherjee A 2012 *Ind. Eng. Chem. Res.* **51** 3740

Sayes C M, Wahi R, Kurian P A, Liu Y, West J L, Ausman K D, Warheit D B and Colvin V L 2006 *Toxicol. Sci.* **92** 174

Schuster K C, Urlaub E and Gapes J R 2000 *J. Microbiol. Meth.* **42** 29

Wang H and Joseph J A 1999 *Free Radical Biol. Med.* **27** 612

Wang T, Bai J, Jiang X and Nienhaus G U 2012 *ACS Nano.* **6** 1251

Zhang H *et al* 2012 *ACS Nano*. **6** 4349

Zhu X, Wang J, Zhang X, Chang Y and Chen Y 2010 *Chemosphere* **79** 928

Zhukova L V, Kiwi J V and Nikandrov V 2010 *Dokl. Chem.* **435** 279